ChemComm

COMMUNICATION

View Article Online
View Journal | View Issue

Cite this: *Chem. Commun.*, 2023, 59, 920

Received 26th November 2022,
Accepted 15th December 2022

DOI: 10.1039/d2cc06408a

rsc.li/chemcomm

Three-dimensional narrow-bandgap perovskite semiconductor ferroelectric methylphosphonium tin triiodide for potential photovoltaic application†

Han-Yue Zhang * and Ren-Gen Xiong

A novel A-site three-dimensional organic–inorganic halide perovskites (3D OIHP) ferroelectric, methylphosphonium tin triiodide ($MPSnI_3$), featuring a narrow bandgap of 1.43 eV, was synthesized. The integration of ferroelectricity with initially moderate efficiency (2.23%) may afford a promising platform to investigate the ferroelectric photovoltaic effect in organic–inorganic halide perovskite solar cells.

The superior performance of methylammonium lead iodide ($MAPbI_3$) in photovoltaic applications is a milestone achievement in perovskite chemistry. It has provoked booming research on organic–inorganic halide perovskites (OIHPs).[1,2] OIHP structures containing organic cations and inorganic frameworks combine the merits of easy processability of solutions, lightweight, highly structural tunability, and additional functionalities.[3–5] These features render OIHPs prominent performance in light-emitting diodes, solar cells, optoelectronic detectors, and ferroelectric devices.[6,7] Three-dimensional (3D) ABX_3 OIHPs (A = organic cations, B = metal, X = halogen), in which A-cations occupy the voids between BX_6 octahedra (most notably (MA or FA)(Pb or Sn)(I or Br)$_3$ where FA is formamidinium), are considered "superstar materials" in optoelectronics and photovoltaics.[8] During the past decade, the power conversion efficiency (PCE) of $MAPbI_3$-based perovskite solar cells (PSCs) has improved from 3.8% to >25%.[9–11] More recently, Zhan and colleagues converted α-$FAPbI_3$ films into PSCs with an efficiency of >23%,[12] comparable with that of commercialized crystalline silicon and GaAs solar cells. Besides the appropriate bandgaps (~1.5 eV) close to the optimal bandgap (~1.34 eV),[10,12] the high photovoltaic performance of $MAPbI_3$ is deemed to be associated to its polar nature and ferroelectric polarization at room temperature.[13–15]

State Key Laboratory of Bioelectronics, School of Biological Science and Medical Engineering, Southeast University, Nanjing 210096, P. R. China.
E-mail: zhanghanyue@seu.edu.cn

† Electronic supplementary information (ESI) available: Materials and methods, NMR, crystal data, PFM, and solar cells. CCDC 2031849–2031850 and 2036182. For ESI and crystallographic data in CIF or other electronic format see DOI: https://doi.org/10.1039/d2cc06408a

Ferroelectric materials with intrinsic spontaneous polarization in photovoltaic devices contribute significantly to formation of a strong local built-in field to facilitate effective separation of electron-hole pairs that are similar to the p–n junctions in conventional solar cells.[16,17] Hence, a ferroelectric photovoltaic effect has long been expected to be a preferable choice for conversion of solar energy. However, the low absorption coefficient and wide bandgap in conventional ferroelectric materials (*e.g.*, BTO, PZT, and $LiNbO_3$) are unacceptable in photovoltaic research.[18] Therefore, ferroelectric materials with a narrow bandgap are very important for high-efficiency photovoltaic devices. $BiFeO_3$ has a small bandgap and can absorb many photons, but large leakage currents caused by ineluctable Fe^{2+} and oxygen vacancies seriously affect ferroelectric polarization.[17,19,20] In OIHPs, Pb-based PSCs have toxic effects on the body and environment. In the past few years, the most promising Sn-based OIHPs have been investigated intensively for applications of solar cells, but they must be lead-free and realize comparable visible-light absorption. Unfortunately, their photovoltaic performances are far from those of lead-based devices.[21–32] FA(Pb or Sn)(I or Br)$_3$ and $MAPbBr_3$ crystallize in centrosymmetric space groups at room temperature and fail to meet the polar symmetry for ferroelectrics.[33–35] In recent years, extensive research has been conducted to extend the family of functional OIHPs,[4,36] whereas the development of new photovoltaic OIHPs has stalled because of the difficulties in stabilizing the parent 3D structural motif. Subjected to the Goldschmidt tolerance factor t ($0.8 < t < 1$), 3D BX_3^- cubic frameworks can accommodate only a few small cations, MA, and FA to support a photoactive black perovskite phase.[37,38] At this stage of their development, construction of 3D OIHP ferroelectrics with new A-site cations seems an incredible challenge.

Phosphonium-based molecules are promising as A-site cations because the P atom and N atom (which belong to the same group in the Periodic Table) have similar covalent characteristics. Thus, phosphonium cations and ammonium cations can enable materials to have similar structures and functions, whereas their differences in atomic radius, mass, electron structure, and bond

length may elicit interesting variables in physical and chemical properties. Based on theoretical calculations of the tolerance factor rule, the methylphosphonium (MP^+) cation has been predicted to be available to fill a 3D cage, thereby meeting the demand for the formation of a stable 3D OIHP structure.[39] Very recently, we synthesized a 3D perovskite molecular ferroelectric $MPSnBr_3$. At the experimental level we showed (for the first time) that MP^+ can serve as a stable A-site cation in OIHPs.[40] Moreover, in 1999, Mitzi *et al.* demonstrated the conducting property of tin iodide frameworks.[41,42] In view of those observations, we synthesized a new 3D lead-free OIHP: methylphosphonium tin iodide ($MPSnI_3$). It features a narrow bandgap (1.43 eV), which is close to the optimal bandgap ($\sim$1.34 eV), thereby making it a competitive candidate for photovoltaic and optoelectronic applications. $MPSnI_3$ is also a multiaxial ferroelectric with a Curie temperature (T_c) of 298 K. These attributes may boost the photoelectric performance of $MPSnI_3$-based solar cells. Compared with $MPSnBr_3$, substituting bromine for iodine: (i) heralded a new structure; (ii) resulted in a black perovskite phase with a narrower bandgap; (iii) broke through the long-term limitation of A-site 3D iodide perovskite species. We believe our discoveries afford a promising platform to investigate the ferroelectric photovoltaic effect in OIHP solar cells and other optoelectronic applications.

We prepared crystals of $MPSnI_3$ in a hydroiodic acid solution of equimolar SnI_2 and MPI (Fig. S1–S3, ESI†). Single-crystal structure studies revealed that $MPSnI_3$ adopted a 3D ABX_3 OIHP structure (A = MP^+, B = Sn^{2+}, and X = I^-), in which organic MP^+ cations were located in 3D-framework cavities surrounded by SnI_6 octahedra, isostructural to the 3D $MASnI_3$ (Fig. 1). The crystal structure of MPI adopted a monoclinic space group $P2_1/m$ (Fig. S4 and Table S1, ESI†).

At 273 K, $MPSnI_3$ crystallized in polar space group *Pba*2 (point group = *mm*2) (Table S1, ESI†). This corresponded to the low-temperature ferroelectric phase (LFP). In the LFP, the MP^+ cations located on 2-fold symmetry axes in the lattice and thus showed 2-fold orientational disorder (Fig. 1a and c). The SnI_6 octahedron was distorted, showing short (average of 3.057(5) Å) and long (average of 3.306(5) Å) Sn–I interatomic distances, and an angle of Sn–I–Sn between 158.9° and 178.0° (Fig. S5a and Table S2, ESI†). At 313 K (high-temperature paraelectric phase (HPP)), the crystal structure of $MPSnI_3$ was refined to the non-centrosymmetric cubic space group $P\bar{4}3m$ (point group $\bar{4}3m$) (Table S1, ESI†) based on the significant piezoelectric signal response by piezoresponse force microscopy (PFM) (Fig. S6, ESI†). Also, MP cations were modelled to be highly disordered spheres to satisfy the cubic symmetry (Fig. 1b and d). The SnI_6 octahedron also changed to a regular octahedron with only one type of Sn–I interatomic distance of 3.1732(1) Å, and the Sn–I–Sn angle became 180.0° (Fig. S5b and Table S2, ESI†). Therefore, the ferroelectric phase transition from LFP to HPP was associated with the order–disorder transition of MP^+ cations and deformation of the $[SnI_3]^-$ framework. According to the Aizu rule, this phase transition in $MPSnI_3$ should be ferroelectric with Aizu notion $\bar{4}3mFmm2$.[43]

Differential scanning calorimetry (DSC) was undertaken to detect the phase transition. During heating, an endothermic peak around 298 K revealed a phase transition for $MPSnI_3$, which was higher by 25 K than that for $MASnI_3$ (Fig. 2a). We confirmed the phase transition by the temperature-dependent second-harmonic generation (SHG) response (Fig. 2b). $MPSnI_3$ exhibited clear SHG signals in the ferroelectric phase. The SHG intensity of $MPSnI_3$ had a marked change in T_c, indicating the appearance of significant symmetry breakage and in accordance with the transition of non-centrosymmetric *mm*2 and $\bar{4}3m$ crystallographic symmetry in ferroelectric and paraelectric phases. However, a change in SHG signal was not observed before or after the phase transition temperature (T_c = 273 K) for $MASnI_3$. We also confirmed the phase transition of $MPSnI_3$ by the dielectric anomaly around T_c in the temperature-dependent dielectric real part (ε') (Fig. 2c). The huge variation of ε' around T_c revealed the ferroelectric-to-paraelectric phase transition for

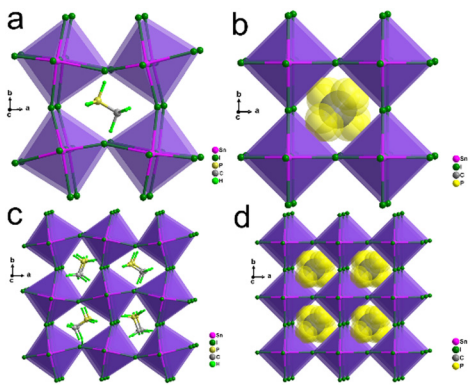

Fig. 1 Basic structures for $MPSnI_3$ at (a) 273 K, and (b) 313 K, respectively. The P atom and C atom of the MP cation are disordered over the two possible positions. Only one distribution is illustrated for clarity. Packing view of the structures for $MPSnI_3$ at (c) 273 K, and (d) 313 K, respectively. H atoms of the organic cations in HPP were not modeled because of total disorder, and thus not shown in (b) or (d).

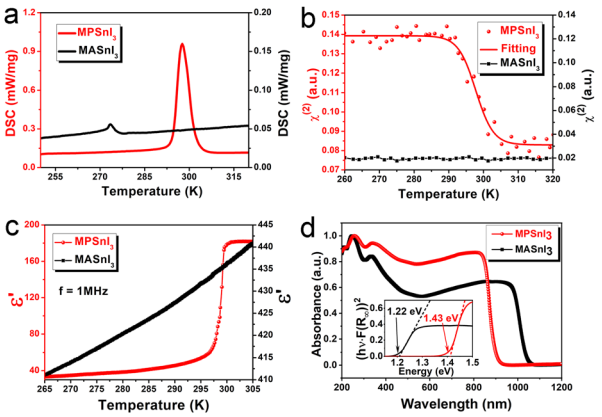

Fig. 2 (a) DSC measurements revealed a structural phase transition at around T_c = 298 K ($MPSnI_3$) and T_c = 273 K ($MASnI_3$). (b) Second-order nonlinear optical coefficient $\chi^{(2)}$ as a function of temperature. (c) Temperature dependence of the real part (ε') of the complex dielectric constant at 1 MHz. (d) Ultraviolet-visible absorption spectra for $MPSnI_3$ and $MASnI_3$. The inset shows the Tauc plot.

$MPSnI_3$. The Curie–Weiss law is not applicable in such an inappropriate ferroelectric compound.[7] The behavior of dielectric permittivity around T_c can be explained by a fitted model based on the Landau–Ginzburg theory (Fig. S7, ESI†).

The optical property of a $MPSnI_3$ crystal was investigated by solid-state UV-vis diffuse reflectance spectroscopy at room temperature. The UV-vis absorbance spectrum displayed intense absorption at a band-edge onset of 900 nm (Fig. 2d). The feature of a direct bandgap semiconductor could be concluded (Fig. 2d, insert). From the *Tauc* plot, the measured optical bandgap for the direct transition was 1.43 eV, which is slightly higher than that for the 3D analogue: $MASnI_3$ (1.22 eV).

To characterize the ferroelectricity of $MPSnI_3$, we employed PFM to enable non-destructive visualization and control of ferroelectric domains on single crystals at 288 K. The clear-domain phase contrast and domain wall are shown in Fig. S3a and S3b (ESI†). The domain structure did not overlap with the topography (Fig. S8, ESI†). For $MPSnI_3$, 180° and non-180° domains could coexist on a single crystal, thereby demonstrating the multiaxial nature (Fig. S9, ESI†).

These stable polarizations in the domains could also be switchable under an external electric field. Fig. 3c and d display the well-defined hysteresis loops and typical butterfly-shaped curves for the vertical phase and amplitude signals *versus* DC bias, respectively, which confirmed the switchable polarization of $MPSnI_3$. We also undertook PFM tip poling experiments to observe domain switching directly. Switched domain patterns could be written on a single crystal of $MPSnI_3$ under application of opposite voltages, which provided solid evidence for ferroelectric polarization switching (Fig. S10, ESI†).[44,45]

We calculated the hypothetical molecular rotation of MA and MP in the inorganic SnI_3^- framework, respectively (Fig. S11, ESI†). The state with the lowest energy emerged at 45° and 135° (Fig. 4a), so the molecule was most stable in the face-center direction, in accordance with the measured crystal structure. Compared with MA cations, the energy barrier of MP rotation was much higher, suggesting a higher ferroelectric phase-transition temperature. Such a high barrier for rotational energy of $MPSnI_3$ may originate from a heavier molecular mass and larger molecular volume.

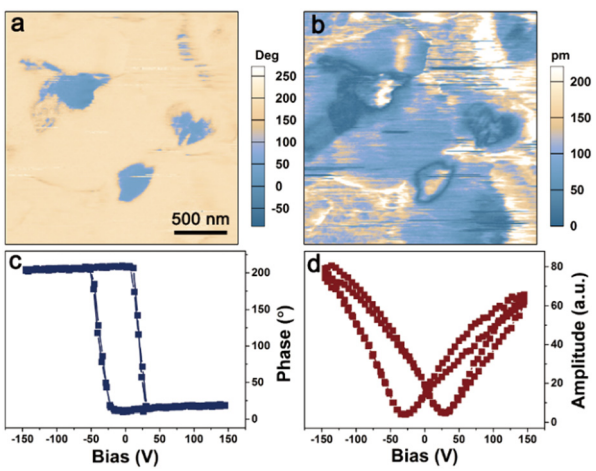

Fig. 3 Vertical PFM phase (a) and amplitude (b) images on the crystal surface of $MPSnI_3$ at 288 K. Vertical PFM phase (c) and amplitude (d) signals *versus* the tip bias at a selected location.

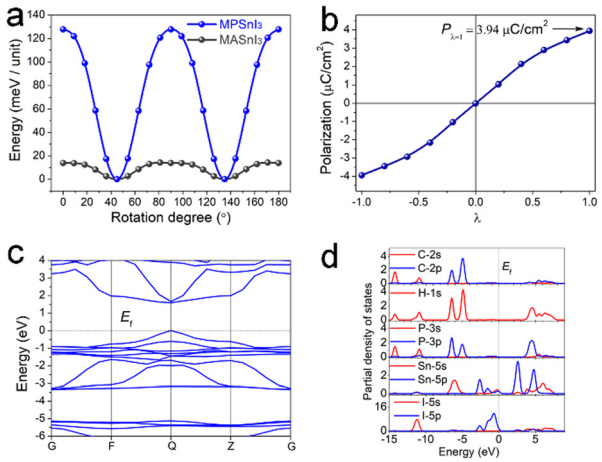

Fig. 4 (a) Rotational energy barrier of MP and MA cations in the inorganic SnI_3^- framework. (b) Evolution path of polarization with structural distortion of $MPSnI_3$. (c) The energy-band structure of a $MPSnI_3$ crystal shows a direct bandgap of 1.58 eV. (d) The partial density of states (PDOS) of a $MPSnI_3$ crystal.

To gain deep insight into ferroelectric polarization reversal, density functional theory (DFT) calculations were carried out to evaluate the origin of polarization.[46,47] Based on the modern theory of polarization,[48,49] a dynamic path between two ferroelectric states is constructed according to the crystal structure acquired from single-crystal X-ray diffraction.

Considering the rotational and displacive motion of MP cations in the anionic SnI_3^- framework, the other states were obtained from the matrix transformation of the coordinates. The variation of polarization *versus* the dynamic path is displayed in Fig. 4b, from which the ferroelectric polarization with 3.94 μC cm^{-2} could be extracted from two equivalent ferroelectric configurations ($\lambda = \pm 1$). During ferroelectric switching ($-1 < \lambda < 1$), the polarization value changed smoothly, and turned to zero at $\lambda = 0$, suggesting a reference phase with zero polarization.

We also calculated the band structure to obtain deep insight into the electronic structure of $MPSnI_3$ (Fig. 4c). The conduction band (CB) minimum and valence band (VB) maximum were localized at the same *k*-vector in the Brillouin zone, so $MPSnI_3$ was a direct bandgap semiconductor, in good agreement with experimental phenomena. The calculated bandgap was 1.58 eV, close to the experimental value of 1.43 eV. Furthermore, bands can be assigned according to the partial density of states (PDOS), as plotted in Fig. 4d. From PDOS, the bands at the top of the VB originated from the nonbonding states of I-5p, and those at the CB bottom were mainly from the unoccupied Sn-5p orbitals. Clearly, the bandgap of the material was determined by the inorganic $\{SnI_3\}^-$ framework.

We conducted preliminary device fabrication to test the photovoltaic performance of $MPSnI_3$ with a device structure of ITO/PEDOT:PSS/perovskite/C60/BCP/Ag (Fig. S12–S17 and Table S3, ESI†). Benefiting from outstanding ferroelectric and semiconductor

properties, the manufactured $MPSnI_3$-based solar-cell device showed initial photoelectric performance, and achieved a moderate PCE of 2.231%.

In summary, we reported a new 3D lead-free OIHP ferroelectric semiconductor of $MPSnI_3$ that showed clear ferroelectricity with a T_c of 298 K and a narrow bandgap of 1.43 eV. $MPSnI_3$ was a multiaxial ferroelectric with the Aizu notion of $\bar{4}3mFmm2$, and the ferroelectric domains and polarization switching confirmed its ferroelectricity. The considerable initial energy conversion efficiency, combined with easy processing of solutions, suggests that $MPSnI_3$ has great potential for photovoltaic, photoelectric, and ferroelectric applications.

We thank Professor Yiqiang Zhan and his co-workers (Fudan University) for their significant contribution to photoelectric experiments. This work was supported by the seventh Youth Elite Scientist Sponsorship Program by the China Association for Science and Technology, the Ten Science and Technology Problem of Southeast University, and the National Natural Science Foundation of China (21991142 and 21831004).

Conflicts of interest

There are no conflicts to declare.

Notes and references

1 M. A. Green, A. Ho-Baillie and H. J. Snaith, *Nat. Photonics*, 2014, **8**, 506–514.
2 J. Y. Kim, J.-W. Lee, H. S. Jung, H. Shin and N.-G. Park, *Chem. Rev.*, 2020, **120**, 7867–7918.
3 C. C. Stoumpos, C. D. Malliakas and M. G. Kanatzidis, *Inorg. Chem.*, 2013, **52**, 9019–9038.
4 W. Li, Z. Wang, F. Deschler, S. Gao, R. H. Friend and A. K. Cheetham, *Nat. Rev. Mater.*, 2017, **2**, 16099.
5 M. Konstantakou and T. Stergiopoulos, *J. Mater. Chem. A*, 2017, **5**, 11518–11549.
6 K. Liu, Y. Jiang, Y. Jiang, Y. Guo, Y. Liu and E. Nakamura, *J. Am. Chem. Soc.*, 2019, **141**, 1406–1414.
7 Y.-M. You, W.-Q. Liao, D. Zhao, H.-Y. Ye, Y. Zhang, Q. Zhou, X. Niu, J. Wang, P.-F. Li, D.-W. Fu, Z. Wang, S. Gao, K. Yang, J.-M. Liu, J. Li, Y. Yan and R.-G. Xiong, *Science*, 2017, **357**, 306–309.
8 A. K. Jena, A. Kulkarni and T. Miyasaka, *Chem. Rev.*, 2019, **119**, 3036–3103.
9 J. Tong, Z. Song, D. H. Kim, X. Chen, C. Chen, A. F. Palmstrom, P. F. Ndione, M. O. Reese, S. P. Dunfield, O. G. Reid, J. Liu, F. Zhang, S. P. Harvey, Z. Li, S. T. Christensen, G. Teeter, D. Zhao, M. M. Al-Jassim, M. F. A. M. van Hest, M. C. Beard, S. E. Shaheen, J. J. Berry, Y. Yan and K. Zhu, *Science*, 2019, **364**, 475–479.
10 H. J. Snaith, *Nat. Mater.*, 2018, **17**, 372–376.
11 A. Kojima, K. Teshima, Y. Shirai and T. Miyasaka, *J. Am. Chem. Soc.*, 2009, **131**, 6050–6051.
12 H. Lu, Y. Liu, P. Ahlawat, A. Mishra, W. R. Tress, F. T. Eickemeyer, Y. Yang, F. Fu, Z. Wang, C. E. Avalos, B. I. Carlsen, A. Agarwalla, X. Zhang, X. Li, Y. Zhan, S. M. Zakeeruddin, L. Emsley, U. Rothlisberger, L. Zheng, A. Hagfeldt and M. Grätzel, *Science*, 2020, **370**, eabb8985.
13 B. Chen, J. Shi, X. Zheng, Y. Zhou, K. Zhu and S. Priya, *J. Mater. Chem. A*, 2015, **3**, 7699–7705.
14 H. Röhm, T. Leonhard, A. D. Schulz, S. Wagner, M. J. Hoffmann and A. Colsmann, *Adv. Mater.*, 2019, **31**, 1806661.
15 J. Breternitz, F. Lehmann, S. A. Barnett, H. Nowell and S. Schorr, *Angew. Chem., Int. Ed.*, 2020, **59**, 424–428.
16 C. Baeumer, D. Saldana-Greco, J. M. P. Martirez, A. M. Rappe, M. Shim and L. W. Martin, *Nat. Commun.*, 2015, **6**, 6136.
17 T. Choi, S. Lee, Y. J. Choi, V. Kiryukhin and S.-W. Cheong, *Science*, 2009, **324**, 63–66.
18 X. Han, Y. Ji and Y. Yang, *Adv. Funct. Mater.*, 2022, **32**, 2109625.
19 T. Rojac, A. Bencan, B. Malic, G. Tutuncu, J. L. Jones, J. E. Daniels and D. Damjanovic, *J. Am. Ceram. Soc.*, 2014, **97**, 1993–2011.
20 Y. B. Yuan, Z. G. Xiao, B. Yang and J. S. Huang, *J. Mater. Chem. A*, 2014, **2**, 6027–6041.
21 Z. Shi, J. Guo, Y. Chen, Q. Li, Y. Pan, H. Zhang, Y. Xia and W. Huang, *Adv. Mater.*, 2017, **29**, 1605005.
22 C. C. Stoumpos and M. G. Kanatzidis, *Acc. Chem. Res.*, 2015, **48**, 2791–2802.
23 B. Lee, C. C. Stoumpos, N. J. Zhou, F. Hao, C. Malliakas, C. Y. Yeh, T. J. Marks, M. G. Kanatzidis and R. P. H. Chang, *J. Am. Chem. Soc.*, 2014, **136**, 15379–15385.
24 S. J. Lee, S. S. Shin, Y. C. Kim, D. Kim, T. K. Ahn, J. H. Noh, J. Seo and S. I. Seok, *J. Am. Chem. Soc.*, 2016, **138**, 3974–3977.
25 S. Y. Shao, J. Liu, G. Portale, H. H. Fang, G. R. Blake, G. H. ten Brink, L. J. A. Koster and M. A. Loi, *Adv. Energy Mater.*, 2018, **8**, 1702019.
26 F. Hao, C. C. Stoumpos, D. H. Cao, R. P. H. Chang and M. G. Kanatzidis, *Nat. Photonics*, 2014, **8**, 489–494.
27 K. Nishimura, M. A. Kamarudin, D. Hirotani, K. Hamada, Q. Shen, S. Iikubo, T. Minemoto, K. Yoshino and S. Hayase, *Nano Energy*, 2020, **74**, 104858.
28 T. B. Song, T. Yokoyama, S. Aramaki and M. G. Kanatzidis, *ACS Energy Lett.*, 2017, **2**, 897–903.
29 A. Abate, *Joule*, 2017, **1**, 659–664.
30 W. J. Ke and M. G. Kanatzidis, *Nat. Commun.*, 2019, **10**, 965.
31 E. Jokar, C. H. Chien, C. M. Tsai, A. Fathi and E. W. G. Diau, *Adv. Mater.*, 2019, **31**, 1804835.
32 W. J. Ke, C. C. Stoumpos and M. G. Kanatzidis, *Adv. Mater.*, 2019, **31**, 1803230.
33 Y. Dang, Y. Zhou, X. Liu, D. Ju, S. Xia, H. Xia and X. Tao, *Angew. Chem., Int. Ed.*, 2016, **55**, 3447–3450.
34 I. Swainson, L. Chi, J.-H. Her, L. Cranswick, P. Stephens, B. Winkler, D. J. Wilson and V. Milman, *Acta Crystallogr., Sect. B: Struct. Sci., Cryst. Eng. Mater.*, 2010, **66**, 422–429.
35 M. T. Weller, O. J. Weber, J. M. Frost and A. Walsh, *J. Phys. Chem. Lett.*, 2015, **6**, 3209–3212.
36 S. Wang, X. Liu, L. Li, C. Ji, Z. Sun, Z. Wu, M. Hong and J. Luo, *J. Am. Chem. Soc.*, 2019, **141**, 7693–7697.
37 D. Li, J. Shi, Y. Xu, Y. Luo, H. Wu and Q. Meng, *Natl. Sci. Rev.*, 2017, **5**, 559–576.
38 W. A. Dunlap-Shohl, Y. Zhou, N. P. Padture and D. B. Mitzi, *Chem. Rev.*, 2019, **119**, 3193–3295.
39 S. Körbel, M. A. L. Marques and S. Botti, *J. Mater. Chem. A*, 2018, **6**, 6463–6475.
40 H. Y. Zhang, X. G. Chen, Z. X. Zhang, X. J. Song, T. Zhang, Q. Pan, Y. Zhang and R. G. Xiong, *Adv. Mater.*, 2020, **32**, 2005213.
41 D. B. Mitzi, S. Wang, C. A. Feild, C. A. Chess and A. M. Guloy, *Science*, 1995, **267**, 1473–1476.
42 C. R. Kagan, D. B. Mitzi and C. D. Dimitrakopoulos, *Science*, 1999, **286**, 945–947.
43 K. Aizu, *J. Phys. Soc. Jpn.*, 1969, **27**, 387–396.
44 T. Besara, P. Jain, N. S. Dalal, P. L. Kuhns, A. P. Reyes, H. W. Kroto and A. K. Cheetham, *Proc. Natl. Acad. Sci. U. S. A.*, 2011, **108**, 6828–6832.
45 C. Qiu, B. Wang, N. Zhang, S. Zhang, J. Liu, D. Walker, Y. Wang, H. Tian, T. R. Shrout, Z. Xu, L.-Q. Chen and F. Li, *Nature*, 2020, **577**, 350–354.
46 D. Di Sante, A. Stroppa, P. Jain and S. Picozzi, *J. Am. Chem. Soc.*, 2013, **135**, 18126–18130.
47 A. Stroppa, P. Barone, P. Jain, J. M. Perez-Mato and S. Picozzi, *Adv. Mater.*, 2013, **25**, 2284–2290.
48 R. Resta and D. Vanderbilt, in *Physics of Ferroelectrics: A Modern Perspective*, ed. K. M. Rabe, C. H. Ahn and J. M. Triscone, 2007, vol. 105, pp. 31–68.
49 N. A. Spaldin, *J. Solid State Chem.*, 2012, **195**, 2–10.